Bol. Soc. Paran. Mat.
©SPM – E-ISSN-2175-1188
SPM: www.spm.uem.br/bspm

(3s.) **v. 2026 (44) 4** : 1–17.
ISSN-0037-8712
doi:10.5269/bspm.80063

Radiation-Absorbing Chemically Reactive Nanofluid Flow with Heat Generation over a Porous Moving Vertical Plate under MHD and Buoyancy Effects

Akhil A. M., Sreegowrav K. R.*

ABSTRACT: Radiation-Absorbing chemically reactive nanofluid flow with heat generation over a porous moving vertical plate under MHD and buoyancy effects is studied. In this study, a nanofluid ($Cu - H_2O$) and a pure fluid (water) are compared across a moving vertical plate with a porous surface surrounding it. Aligned magnetic force (B_0) effect is applied to the direction of the nanofluid flow. We assume that both the temperature and the concentration remain constant while the plate moves with a constant velocity u_0. In order to solve the governing equations, the Perturbation Technique is employed. This study uses graphs and tables to examine and assess the impacts of several physical parameters, such as the radiation absorption parameter and the heat generation/absorption parameter. Notably, the radiation absorption parameter raises the temperatures, velocities, and shear stresses. Research and discussions have focused on shearing stress, Nusselt number, and Sherwood number.

Key Words: Radiation absorption parameter, MHD, Heat source, porous medium.

Contents

1. Introduction

Engineered colloidal suspensions of nanoparticles in a base fluid typically water or oil are known as nanofluids. These nanoparticles are uniformly distributed throughout the base fluid and usually have diameters of less than 100 nanometers. The basic fluid's thermophysical characteristics, such as its viscosity, thermal conductivity, and heat transfer coefficients, are changed by the addition of nanoparticles. Because of their special qualities, such as increased thermal conductivity, nanofluids are attractive options for a number of uses, such as heat transfer in electrical devices, cooling systems, and solar energy systems. To increase the performance and range of uses of nanofluids, researchers are investigating strategies to enhance their compositions and fabrication techniques. For broad use, nevertheless, issues like the stability of nanoparticles, economic viability, and possible environmental effects must be resolved.

A study comparing nanofluid ($Cu-H_2O$) and pure fluid (water) was conducted by Arulmozhi et al. [1] over a moving vertical plate encircled by a porous surface. In order to get a higher thermal conductivity of

* Corresponding author.
2020 *Mathematics Subject Classification:* 05C50,05C90.
Submitted November 11, 2025. Published February 03, 2026

nanofluid than pure fluid, the study's uniqueness lies in its inclusion of the unstable laminar MHD natural transmission flow of an incompressible fluid. In their study, Prasad et al. [2] examined how a semi-infinite flat plate confined a nanofluid and how radiation absorption, chemical reactions, and diffusion thermal affected the mass transfer flow and MHD free convective heat. Using heat generation/absorption, thermal radiation, and MHD flow of boundary layer, Reddy, P. Y. [3] examined the mass and heat transmission of nanofluids across an inclining vertical plate filled with permeable material. A partially infinite vertical plate in motion was subjected to radiation, hydromagnetism, and temperature oscillations effects in the study by Rajesh et al. [4], which examined the effects of transient free convection flow as well as heat transfer on electrically conducting, viscous, and incompressible nanofluid. Using analytical approaches, Rajesh et al. [5] investigated a hybrid nanofluid motion problem involving heat transfer across an endless flat vertical plate with an escalating temperature gradient with regard to time. In their study, Kumaresan et al. [6] sought to find a precise solution to the following problem: a silver nanofluid is flowing via a porous medium at an abruptly accelerating rate via a vertical plate that is being moved at a longitudinal magnetic field, in the presence of thermal radiation, a transversely applied magnetic field, radiation absorption, and chemical reactions that generate or absorb heat. The MHD-induced convective flow of a nanofluid via a continuous smooth plate surrounded by a porous substance is studied by Pavar et al. [7] in relation to the implications of diffusion-thermo and radiation-absorption. The hydro electromagnetic boundary layer flows through nanofluids when a moving vertical plate is subjected to heat radiation and an evenly distributed longitudinal magnetic field, as shown by Das and Jana [8]. Casson nanofluid free convective flow as well as heat transfer on a plate that is vertical were investigated by Sobamowo [9] in relation to the effects on heat radiation as well as nanoparticles. Considering the impacts of radiation absorption and heat generation, Arifuzzaman et al. [10] conducted a numerical investigation of MHD transitory natural convection and greater-order chemically reacting Maxwell fluid moving through a vertical porous plate containing nanoparticles. When a chemical reaction was present, Prakash et al. [11] investigated how a transversely applied magnetic field affected the inconsistent hydro-magnetic transfer of heat and mass flow of a dense, dusty, incompressible and electrically conducting fluid across two porous, parallel plates that were heated vertically. The fluid was also characterised by its incompressibility. The computational study by Nayan et al. [12] aims to clarify the orientated MHD flow of a hybrid nanofluid across a vertical plate in a porous medium. The researchers Krishna et al. [13] looked into how a constant longitudinal magnetic field as well as heat radiation absorption affected the unstable MHD flow through the boundary layer over a moving vertical permeable surface with nanofluids. When a constant heat flux and an unstable MHD natural convection flow of a viscous fluid subjected to radiation were considered, Haq et al. [14] examined the heat transmission that took place in the scenario of an infinitely vertical plate attached to a porous material. The effect of rotation as well as heat radiation on the chaotic multi-layer stratified convection that occurs via a continuously rotating vertical absorbing plate was studied by Krishna et al. [15]. Researchers Anwar et al. [16] examined a time-varying convection-free water-based flow of nanofluid that carries Cu and TiO_2 particles through a sliding permeable vertical plate. The flow is driven by both electrical and thermal forces. By taking into consideration several sorts of parameters, Rosaidi et al. [17] studied the behaviour of magnetic nanofluids in multi-homogeneous free convection flow on an oscillating vertical plate under convective boundary circumstances. A study conducted by Zukri et al. [18] examined the effects of different nanoparticle geometries on MHD, heat transfer across an oscillating vertical plate under the convective boundary circumstance, and Casson hybrid nanofluid flow. Using a longitudinal magnetic field as well as the thermal soret implications, Raghunath [19] studied the mass and heat exchange of a water-soluble nanofluid (Cu and TiO_2) operating in an unsteady MHD incompressible way across a stretching sheet. A study conducted by Nadeem et al. [20] examined the laminar, two-dimensional flow through the boundary layer of MHD Maxwell nanofluid across a flat porous plate that was moving vertically. A non-Newtonian nanofluid flows over a partially infinitely sliding vertical plate subjected to an externally constant magnetic field, as studied by El-Dabe et al. [21] in their investigation of heat and mass transfer through porous media. In their analysis, Rahman and Uddin [22] considered a nanofluid's incompressible flow through the boundary layer over an endless vertical sheet in the presence of radiation, a changing chemical reaction, and viscosity that depends on temperature. Nanofluid movement and transfer of heat from an endless vertical sheet in the presence of magnetic field, viscous dissipation, and thermal radiation was studied by Kumar et al. [23]

Based on the above facts, in the current study, we conducted numerical and analytical computations on naturally occurring convective, transient, MHD nanofluid flow across an infinite moveable vertical plate under the conditions of uniform suction, chemical reaction, and nonlinear thermal condition. Additionally, a comparative analysis of the velocity, temperature and concentration profiles heat transfer enhancement level brought about by the suspension of $Cu-$water nanofluid ($\phi \neq 0$) and base fluid ($\phi = 0$) is described using graphs and tables. The conclusions that can be evaluated are those that are most in line with the numerical solutions that correspond to the experimental results.

Table 1: Thermophysical attributes of nanofluids (Arulmozhi[1])

Suction	$a_2 = -v_0$
Density	$\rho_{nf} = (1-\phi)\rho_f + \phi\rho_s$
Heat capacity	$(\rho c_p)_{nf} = (1-\phi)(\rho c_p)_f + \phi(\rho c_p)_s$
Thermal expansion (Fluid)	$(\rho\beta)_{nf} = (1-\phi)(\rho\beta)_f + \phi(\rho\beta)_s$
Thermal expansion (Solid)	$(\rho\beta)^*_{nf} = (1-\phi)(\rho\beta)^*_f + \phi(\rho\beta)^*_s$
Viscosity	$\mu_{nf} = \frac{\mu_f}{(1-\phi)^{2.5}}$
Thermal diffusivity	$\alpha_{nf} = \frac{K_{nf}}{(\rho c_p)_{nf}}$
Thermal conductivity	$K_{nf} = K_f \left(\frac{K_s + 2K_f - 2\phi(K_f - K_s)}{K_s + 2K_f + 2\phi(K_f - K_s)} \right)$

Table 2: Thermophysical properties of water and other nanoparticles (Kumaresan [6], Das [8])

Physical properties	**H_2O (water)**	**Cu (copper)**
$\rho\ (kg/m^3)$	997.1	8933
$c_p\ (J/kgK)$	4179	385
$K\ (W/mK)$	0.613	401
$\beta \times 10^{-5}\ (1/K)$	21	1.67
φ	0	0.05

2. Physical model and solution of the problem

In this formulation, an unsteady and incompressible nanofluid moves through a porous medium past an infinitely long vertical surface. The surface itself is in motion, and the nanofluid flows parallel to the direction of the plate's movement. A magnetic field B_0 aligned with the vertical plate is imposed, acting perpendicular to the direction of the fluid flow. Assumptions about the present issue are as follows.

a) In this case, the influence of the pressure gradient is disregarded.

b) The plate is subjected to radiative heat transfer acting in the direction normal to its surface.

c) The base fluid and the dispersed nanoparticles are assumed to be in thermal equilibrium.

d) The density is treated as a linear function of temperature, and the buoyancy effects are incorporated into the momentum equations accordingly.

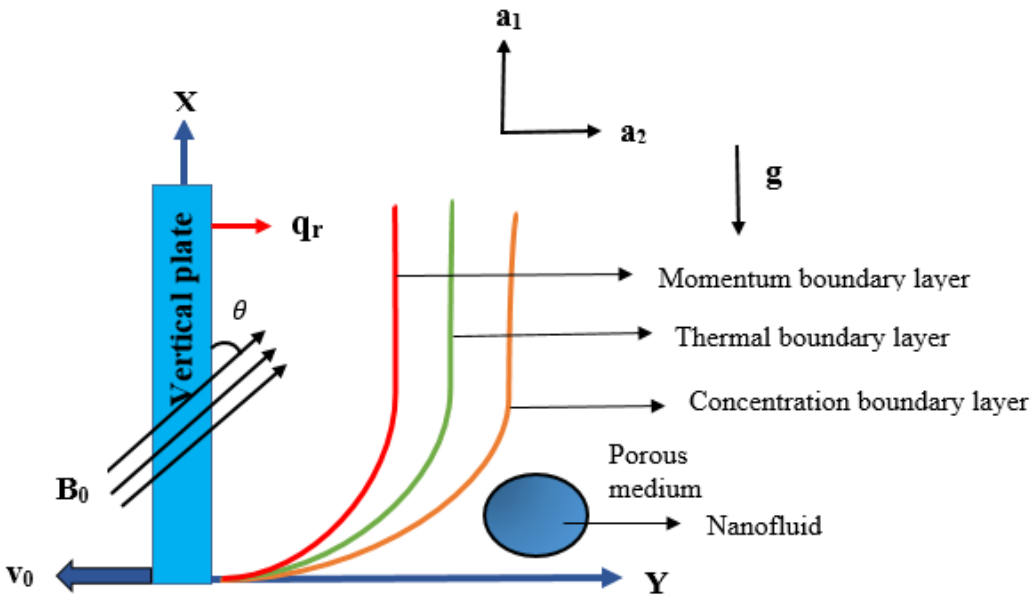

Figure 1: Flow model.

Governing equations

Based on the assumptions mentioned before (Das and Jana [8]), the following can be stated as the momentum, concentration and energy equations for a moving vertical plate subjected to a magnetic field as well as heat radiation: The flow model's portrayal of the flow equation is as follows:

$$\frac{\partial a_2}{\partial y'} = 0, \tag{2.1}$$

$$\rho_{nf}\left(\frac{\partial a_1}{\partial t'} + a_2\frac{\partial a_1}{\partial y'}\right) = \mu_{nf}\frac{\partial^2 a_1}{\partial y'^2} + (\rho\beta)_{nf} g(b_1 - b_{1\infty}) + (\rho\beta)^*_{nf}\, g(c_1 - c_{1\infty}) - \sigma B_0^2 \sin^2\theta a_1 - \frac{\mu_{nf}}{k'} a_1 \tag{2.2}$$

$$\left(\frac{\partial b_1}{\partial t'} + a_2\frac{\partial b_1}{\partial y'}\right) = \alpha_{nf}\frac{\partial^2 b_1}{\partial y'^2} - \frac{1}{(\rho c_p)_{nf}}\frac{\partial q_r}{\partial y'} - \frac{Q\,(b_1 - b_{1\infty})}{(\rho c_p)_{nf}} + \frac{R\,(c_1 - c_{1\infty})}{(\rho c_p)_{nf}} \tag{2.3}$$

$$\left(\frac{\partial c_1}{\partial t'} + a_2\frac{\partial c_1}{\partial y'}\right) = D_B\frac{\partial^2 c_1}{\partial y'^2} - k_r^*\,(c_1 - c_{1\infty}) \tag{2.4}$$

In the present mathematical model, the subsequent boundary conditions are associated (Arulmozhi[1]):
when $t' \leq 0$, at $y' = 0$
$a_1\left(y', t'\right) = 0,$
$b_1\left(y', t'\right) = b_{1\infty},$
$c_1\left(y', t'\right) = c_{1\infty}$
when $t' > 0$, at $y' = 0$ $a_1\left(y', t'\right) = u_0,$
$b_1\left(y', t'\right) = b_{1w} + (b_{1w} - b_{1\infty}) \in e^{iwt},$
$c_1\left(y', t'\right) = c_{1w} + (c_{1w} - c_{1\infty}) \in e^{iwt}$
when $t' > 0$, at $y'_\infty \to \infty$
$a_1\left(y', t'\right) = 0,$

$b_1\left(y^{'},t^{'}\right)=b_{1\infty}$,
$c_1\left(y^{'},t^{'}\right)=c_{1\infty}$
The Rosseland diffusion approximation Hossain [29] and follows Das [8] is applied to get the total radiation heat flux q_r,

$$q_r=\frac{-4\sigma_1}{3K_e}\frac{\partial b_1^4}{\partial y^{'}} \tag{2.5}$$

$$b_1^4\approx 4b_{1\infty}^3b_1-3b_{1\infty}^4 \tag{2.6}$$

If we plug both (2.5) and (2.6) into (2.3), we obtain,

$$\frac{\partial q_r}{\partial y^{'}}=-\frac{16\sigma_1b_{1\infty}^3}{3k_e}\frac{\partial^2 b_1}{\partial y^{1^2}} \tag{2.7}$$

When transforming governing equations into ordinary differential equations (ODEs), dimensionalless variables are as follows:
$U=\frac{a_1}{u_0},y=\frac{u_0y^{'}}{\nu_f},t=\frac{u_0^2t^{'}}{\nu_f},w=\frac{\nu_fw^{'}}{u_0^2},T=\frac{b_1-b_{1\infty}}{b_{1w}-b_{1\infty}},\psi=\frac{c_1-c_{1\infty}}{c_{1w}-c_{1\infty}}$,
$N_r=\frac{16\sigma_1b_{1\infty}^3}{3k_fk_e},G_r=\frac{(\rho\beta)_f\nu_f(b_{1w}-b_{1\infty})g}{\rho_fu_0^3},P_r=\frac{\nu_f}{\alpha_f},S=\frac{v_0}{u_0},S_c=\frac{\nu_f}{D_B},K_r=\frac{K_r^*\nu_f}{u_0^2}$,
$G_m=\frac{(\rho\beta)_f^*\nu_f(c_{1w}-c_{1\infty})g}{\rho_fu_0^3},K=\frac{K^{'}\rho_fu_0^2}{\nu_f^2},M=\frac{\sigma B_0^2\nu_f}{\rho_fu_0^2},\ Q_h=\frac{Q\nu_f^2}{k_fu_0^2},R_a=\frac{R(c_{1w}-c_{1\infty})\nu_f^2}{u_0^2(b_{1w}-b_{1\infty})k_f}$.
The governing equations have been transformed into, by substituting the aforementioned non-dimensional variables into (2.2) to (2.4),

$$A_1\left[\frac{\partial U}{\partial t}-S\frac{\partial U}{\partial y}\right]=\left[E_2\frac{\partial^2U}{\partial y^2}+E_3G_r(T)+E_4G_m(\psi)-\left(M\sin^2\theta+\frac{1}{K}\right)U\right] \tag{2.8}$$

$$\frac{\partial T}{\partial t}-S\frac{\partial T}{\partial y}=\frac{1}{\mathrm{P}_rA}\left[E_1\frac{\partial^2T}{\partial y^2}-Q_hT+R_a\psi\right] \tag{2.9}$$

$$\frac{\partial \psi}{\partial t}-S\frac{\partial \psi}{\partial y}=\frac{1}{S_c}\frac{\partial^2\psi}{\partial y^2}-K_r\psi \tag{2.10}$$

The following are the non-dimensional boundary conditions:

$$\begin{aligned}&t\le 0;U=0,T=0,\psi=0,\forall y\ge 0\\&t>0;U=1,T=1+\in e^{iwt},\psi=1+\in e^{iwt},y=0\\&t>0;U=0,T=0,\psi=0,y\to\infty\end{aligned} \tag{2.11}$$

2.1. Perturbation analysis

By changing the mean steady flow from an unstable one into an ordinary differential equation (ODE), we can solve the non-linear mathematical equations 2.8-2.10.

$$U(y,t)=u_0+\in u_1e^{iwt} \tag{2.12}$$

$$T(y,t)=T_0+\in T_1e^{iwt} \tag{2.13}$$

$$\psi(y,t)=\psi_0+\in \psi_1e^{iwt} \tag{2.14}$$

Equations 2.8-2.10 are shorted to

$$E_2u_0^{''}+A_1Su_0^{'}-\left(M\sin^2\theta+\frac{1}{K}\right)u_0=-E_3G_rT_0-E_4G_m\psi_0 \tag{2.15}$$

$$E_2u_1^{''}+A_1Su_1^{'}-\left(M\sin^2\theta+\frac{1}{K}+A_1iw\right)u_1=-E_3G_rT_1-E_4G_m\psi_1 \tag{2.16}$$

$$E_1 T_0^{''} + P_r A S T_0^{'} - Q_h T_0 = -R_a \psi_0 \tag{2.17}$$

$$E_1 T_1^{''} + P_r A S T_1^{'} - \left[P_r A (iw) + Q_h\right] T_1 = -R_a \psi_1 \tag{2.18}$$

$$\psi_0^{''} + S_c S \psi_0^{'} - K_r S_c \psi_0 = 0 \tag{2.19}$$

$$\psi_1^{''} + S_c S \psi_1^{'} - (iw + K_r) S_c \psi_1 = 0 \tag{2.20}$$

The boundary conditions of equation (2.11) have been transformed into

$$\begin{aligned} &u_0 = 1, u_1 = 0, T_0 = 1, T_1 = 1, \psi_0 = 1, \psi_1 = 1 \text{ at } y = 0, \\ &u_0 = 0, u_1 = 0, T_0 = 0, T_1 = 0, \psi_0 = 0, \psi_1 = 0 \text{ at } y \to \infty, \end{aligned} \tag{2.21}$$

Solving (2.15)-(2.20) then utilising (2.21), we have

$$\begin{aligned} U(y,t) = &\left[(1 - B_3 - B_4 - B_5)\, e^{-m_5 y} + B_3 e^{-m_3 y} + (B_4 + B_5) e^{-m_1 y}\right] \\ &+ \in \left[(-B_6 - B_7 - B_8)\, e^{-(s_5 + i s_6) y} + B_6 e^{-(s_3 + i s_4) y} + (B_7 + B_8) e^{-(s_1 + i s_2) y}\right] e^{iwt}, \end{aligned} \tag{2.22}$$

$$T(y,t) = (1 - B_1) e^{-m_3 y} + B_1 e^{-m_1 y} + \in \left[(1 - B_2) e^{-(s_3 + i s_4) y} + B_2 e^{-(s_1 + i s_2) y}\right] e^{iwt}, \tag{2.23}$$

$$\psi(y,t) = e^{-m_1 y} + \in e^{-(s_1 + s_2) y} e^{iwt}. \tag{2.24}$$

The following equation provides Sherwood number:

$$Sh = -\left(\frac{\partial \psi}{\partial y}\right)_{y=0} = m_1 + \in (s_1 + i s_2)\, e^{iwt}. \tag{2.25}$$

The following equation provides Nusselt number:

$$Nu = -\left(\frac{\partial T}{\partial y}\right)_{y=0} = m_3 (1 - B_1) + m_1 B_1 + \in \left[(1 - B_2)(s_3 + i s_4) + B_2 (s_1 + i s_2)\right] e^{iwt}. \tag{2.26}$$

The following equation provides the shearing stress at the plate:

$$\begin{aligned} \tau = \left(\frac{\partial U}{\partial y}\right)_{y=0} = &\left[-m_5 (1 - B_3 - B_4 - B_5) - m_3 B_3 - m_1 (B_4 + B_5)\right] \\ &+ \in \left[-(s_5 + i s_6)(-B_6 - B_7 - B_8) - (s_3 + i s_4) B_6 - (s_1 + i s_2)(B_7 + B_8)\right] e^{iwt} \end{aligned} \tag{2.27}$$

3. Discussions on the results

In the present work, both analytical and numerical analyses are carried out for transient, natural convection MHD nanofluid flow past an infinitely long, moving vertical plate. The flow is examined under the influences of uniform suction, chemical reaction, and a nonlinear thermal boundary condition. The governing equations are solved using the perturbation method. The impact of several physical parameters–such as the heat generation/absorption parameter and radiation absorption parameter–is explored and demonstrated through graphs and tables for validation. A set of commonly used dimensionless parameters is employed in the formulation. Since equations (2.22), (2.23), and (2.24) yield complex solutions, they are separated into their real and imaginary components, and corresponding graphs are generated for each part. The graphical results are presented in Figures 2 to 19, where subplots (a) and (b) represent the primary and secondary velocity profiles, respectively. The graphs are plotted by assuming parameters as $Qh = 0.5; Ra = 1.5; S = 0.5; Pr = 7; \phi = 0.05; Nr = 1.5; M = 1.5; G_r = 2; G_m = 2; K_r = 0.6; S_c = 0.6; w = \frac{\pi}{6}; K = 2; \epsilon = 0.05$.

3.1. Parameter effects on velocity profiles

Figures 2(a) and 2(b) show velocity profiles of the $Cu - H_2O$ nanofluid for different ϕ . The non-dimensional velocity tends to decrease as ϕ on the $Cu-$nanoparticles rises. Additionally, this figure demonstrates how the velocity steadily drops as y rises. The velocity profiles of the $Cu-$water nanofluid with respect to Qh are shown in Figure 3(a) and 3(b). The velocity profile drops as heat absorption increases and the velocity in the outer layer rises as heat generation increases. When the fluid's velocity is increased due to heat creation, which supplements the fluid's thermal state, the thermal buoyant force is increased. The velocity profiles for various values of Ra are illustrated in Figures 4(a) and 4(b). It shows that when Ra gets larger, the non-dimensional velocity also tends to grow. For one thing, as heat is absorbed, the flow speeds up due to the buoyancy effect. As Ra increases, the buoyancy and temperature and momentum boundary layer thickness also increase, suggesting that conduction is more important than radiation absorption. Figures 5(a) and 5(b) illustrates enhanced surface cooling, as the values of G_r, and G_m rises, the non-dimensional velocity also grows. Figures 6(a) and 6(b) show that the velocity of both nanofluids and pure fluids decreases as M increases. A Lorentz force is generated when an electrical conducting material is subjected to a cross-sectional magnetic field. Figures 7(a) and 7(b) show that increasing values of S result in decreasing velocities of both the nanofluid and the pure fluid. Figures 8(a) and 8(b) explains that higher the chemical reaction parameter (K_r), lesser is the velocity profile. The velocity profile rises with increasing N_r, as seen in Figures 9(a) and 9(b), before falling along y to achieve the free stream velocity.

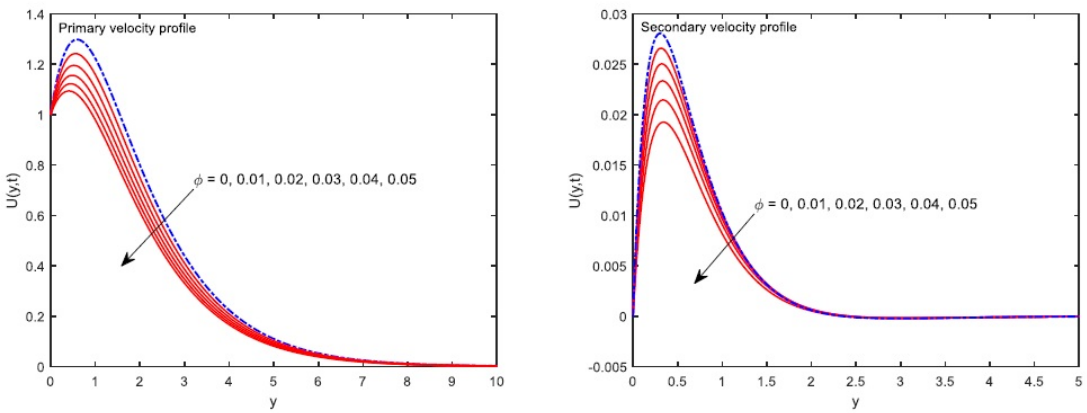

Figure 2: (a) and (b) velocity distributions in $Cu-$water for different ϕ

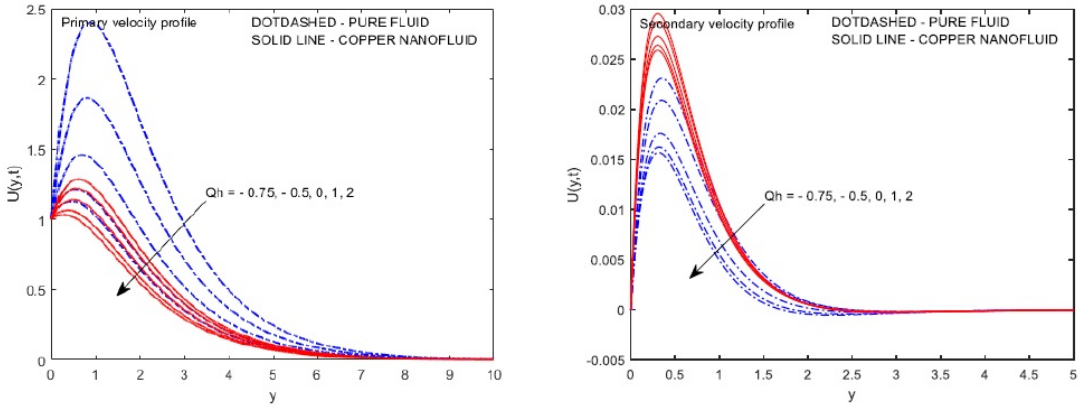

Figure 3: (a) and (b) velocity distributions in $Cu-$water for different Qh

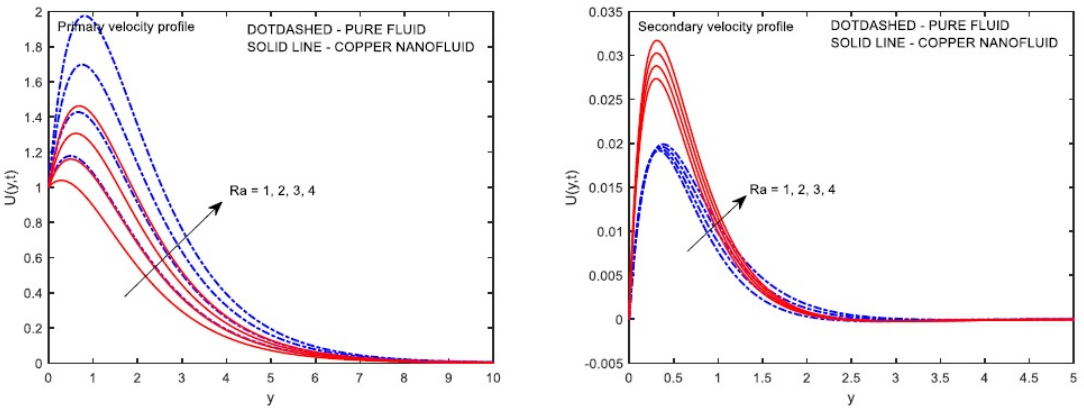

Figure 4: (a) and (b) velocity distributions in $Cu-$water for different Ra

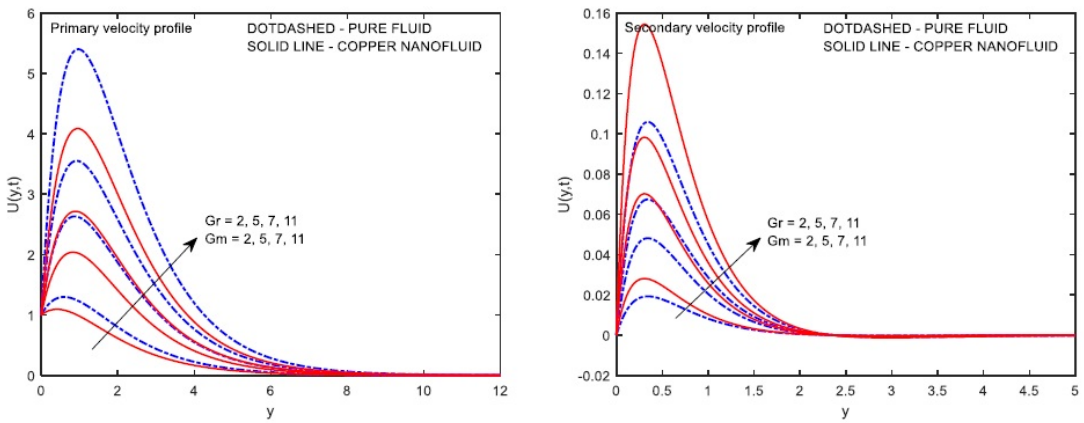

Figure 5: (a) and (b) velocity distributions in $Cu-$water for different G_r and G_m

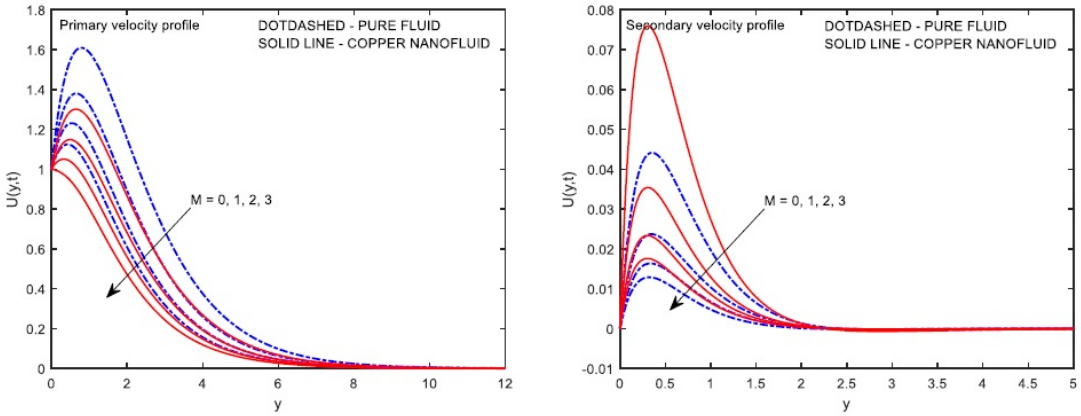

Figure 6: (a) and (b) velocity distributions in $Cu-$water for different M

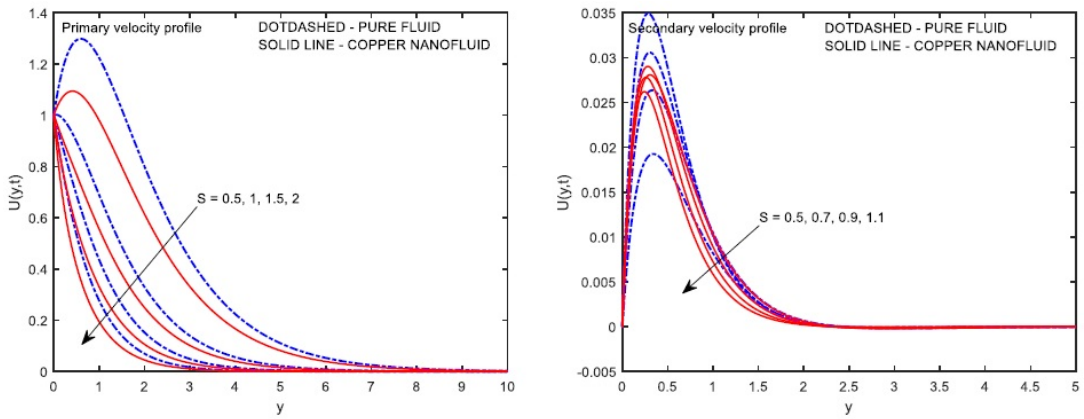

Figure 7: (a) and (b) velocity distributions in $Cu-$water for different S

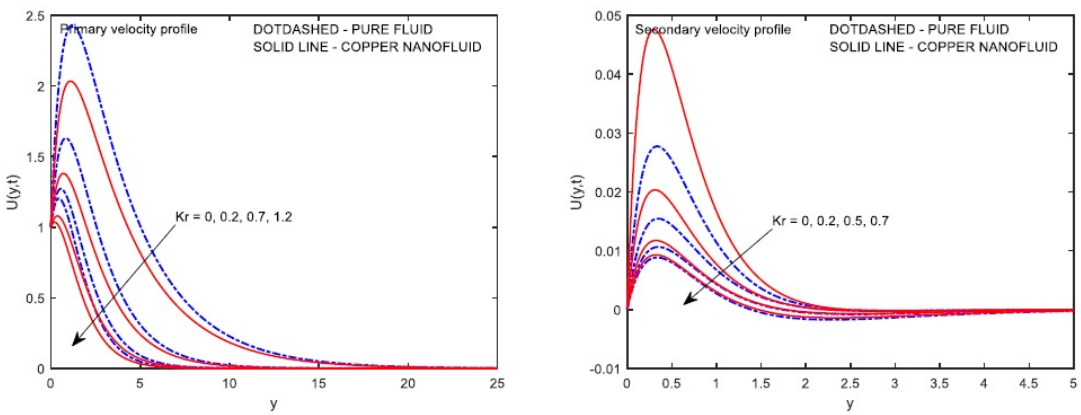

Figure 8: (a) and (b) velocity distributions in $Cu-$water for different K_r

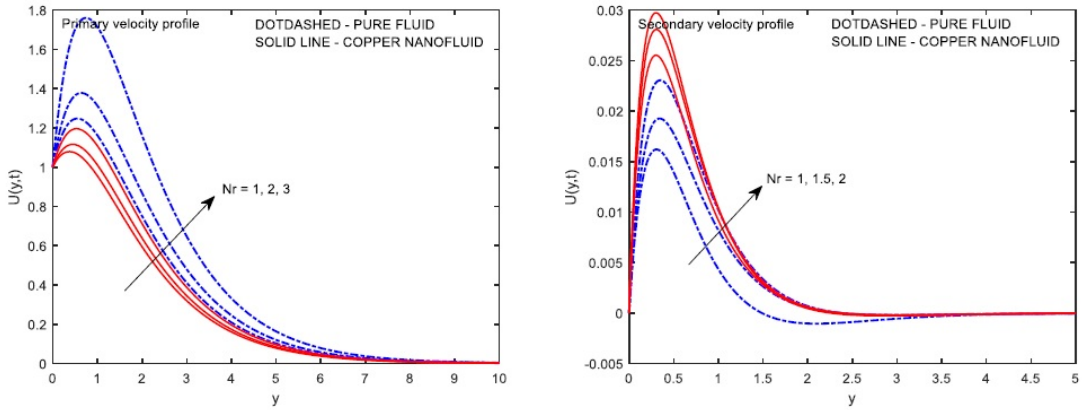

Figure 9: (a) and (b) velocity distributions in $Cu-$water for different N_r

3.2. Parameter effects on temperature profiles

Figures 10(a) and 10(b) show the temperature distribution of $Cu-$water nanofluid plotted against the influence of ϕ. It explains how the temperature drops rapidly as ϕ increases. The temperature profile is enhanced by the rising solid volume fraction because the inclusion of nanoparticles improves thermal conductivity. Figures 11(a) and 11(b) illustrates the temperature profiles of $Cu-$water nanofluid with various values of Qh. Increased heat absorption results in a lower temperature, whereas increased heat generation raises the temperature in the boundary layer. Figures 12(a) and 12(b) show the temperature distributions for various Ra values. As Ra levels grow, it becomes clear that the temperature is rising. This occurs because the absorption of heat causes the effect of buoyancy to speed up the flow. The temperature profiles of the nanofluid and pure fluid decrease as the levels of S increase, as shown in Figure 13(a) and 13(b). The temperature distribution drops as K_r rises, as seen in Figures 14(a) and 14(b). Figures 15(a) and 15(b) show that as N_r increases, the temperature distribution goes up. This is because a higher radiation level results in a larger heat flux, which in turn makes the boundary layer hotter. Once it hits the temperature of the free stream, the temperature drops continuously.

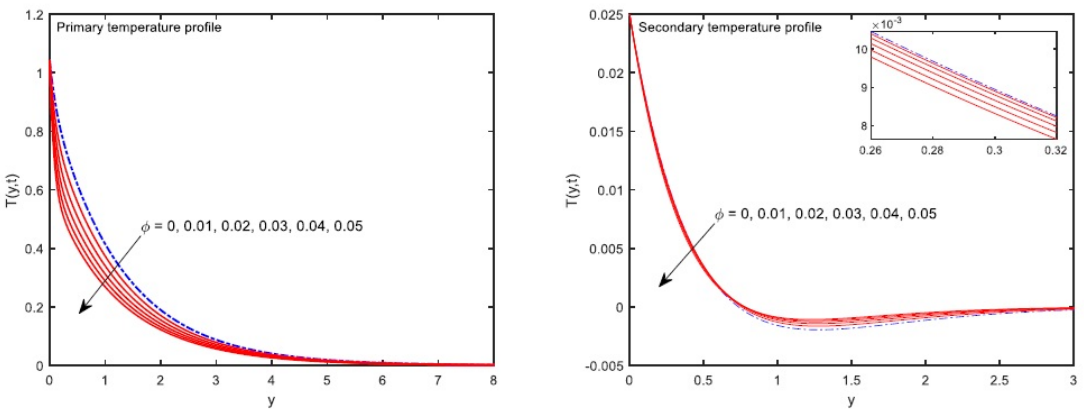

Figure 10: (a) and (b) temperature distributions in $Cu-$water for different ϕ

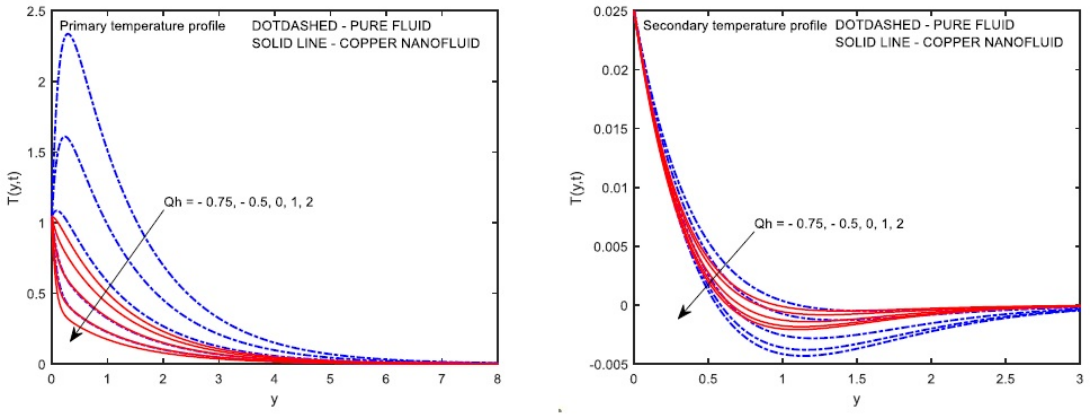

Figure 11: (a) and (b) temperature distributions in $Cu-$water for different Qh

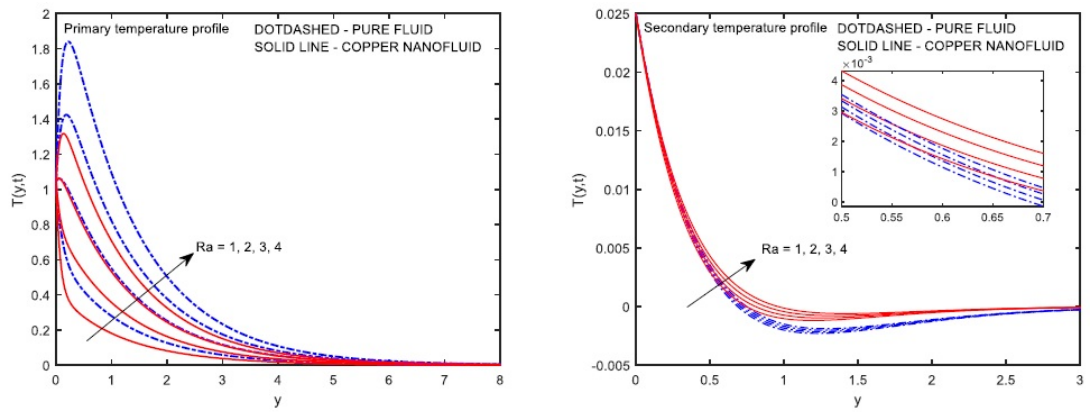

Figure 12: (a) and (b) temperature distributions in $Cu-$water for different Ra

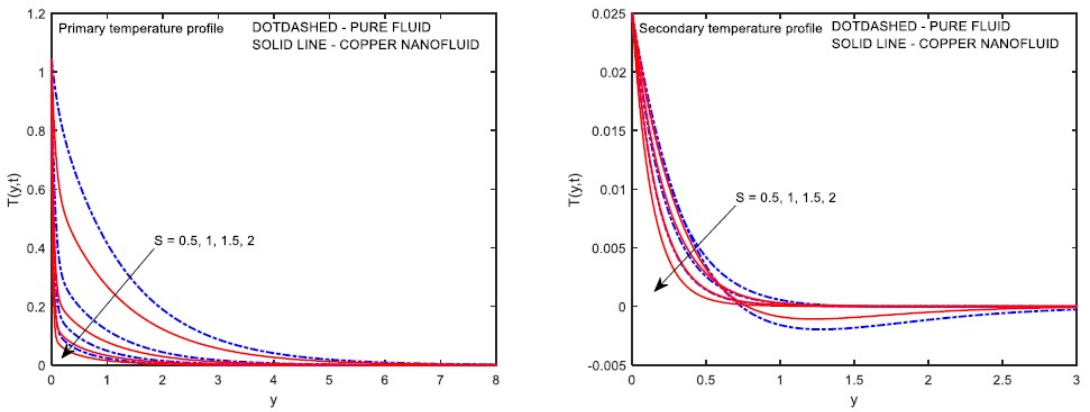

Figure 13: (a) and (b) temperature distributions in $Cu-$water for different S

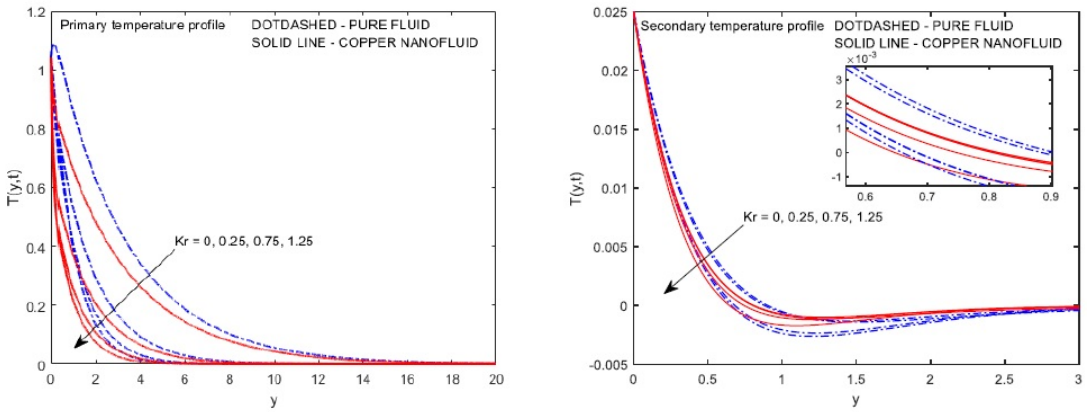

Figure 14: (a) and (b) temperature distributions in $Cu-$water for different K_r

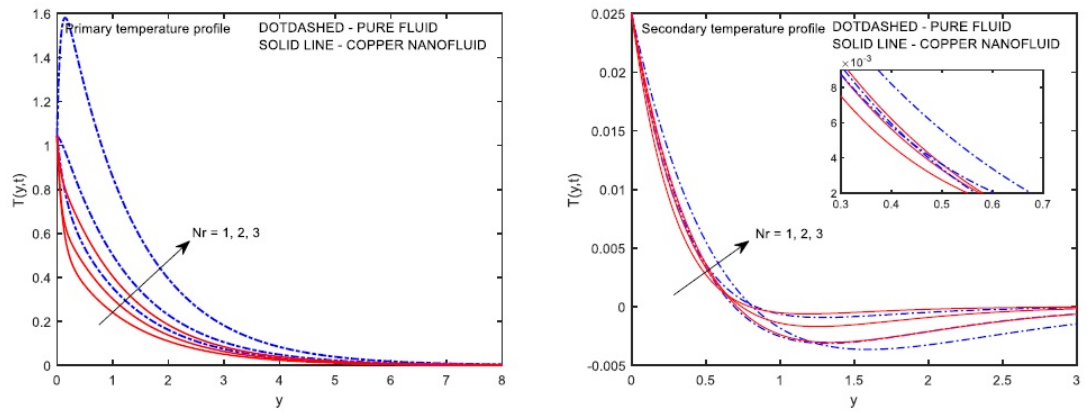

Figure 15: (a) and (b) temperature distributions in $Cu-$water for different N_r

3.3. Parameter effects on concentration profiles

The effect of S on the concentration distribution of the $Cu-$water nanofluid is shown in Figures 16(a) and 16(b), which are plotted. As the concentration of the suction parameter increases, the solubility limit layer's thickness decreases. Figures 17(a) and 17(b) reveal that the higher the value of K_r, the lower its concentration.

The numerical values of the Sherwood number, the Nusselt number, and the shearing stress for several types of nanofluids are presented in Tables 3, 4, and 5. The Sherwood number increases as the values of S and K_r increase, as shown in table 3. Table 4 shows that as S, K_r, and Qh increase, the Nusselt number increases, but as Ra and N_r decrease, the Nusselt number decreases. According to table 5, when the values of S, K_r, Qh, and M increase, the shear stress decreases, but the shear stress increases for G_r, G_m, Ra and N_r.

Table 3: The Sherwood number and its numerical values

S	K_r	**Sherwood number** $(Cu - H_2O)$
1	0.6	1.0524
2	0.6	1.5711
3	0.6	2.1505
4	0.6	2.7593
0.5	**1**	1.0175
0.5	**2**	1.3617
0.5	**3**	1.6274
0.5	**4**	1.8520

Table 4: Variation of Nusselt number with different parameters for $Cu - H_2O$ nanofluid

S	K_r	N_r	Qh	Ra	Nu $(Cu - H_20)$
0.5	0.6	1.5	0.5	1.5	6.5946
1	0.6	1.5	0.5	1.5	21.8860
1	0.6	1.5	0.5	1.5	36.2892
2	0.6	1.5	0.5	1.5	50.3713
0.5	**0**	1.5	0.5	1.5	2.1364
0.5	**0.25**	1.5	0.5	1.5	5.6629
0.5	**0.75**	1.5	0.5	1.5	6.7341
0.5	**1.25**	1.5	0.5	1.5	6.7453
0.5	0.6	**1**	0.5	1.5	6.0415
0.5	0.6	**2**	0.5	1.5	6.6381
0.5	0.6	**3**	0.5	1.5	4.0712
0.5	0.6	1.5	**-0.75**	1.5	0.0414
0.5	0.6	1.5	**-0.5**	1.5	1.9104
0.5	0.6	1.5	**0**	1.5	4.6320
0.5	0.6	1.5	**1**	1.5	8.1299
0.5	0.6	1.5	**2**	1.5	10.4778
0.5	0.6	1.5	0.5	**1**	9.0984
0.5	0.6	1.5	0.5	**2**	4.0908
0.5	0.6	1.5	0.5	**3**	-0.9168
0.5	0.6	1.5	0.5	**4**	-5.9243

Table 5: The shearing stress and its numerical values

S	K_r	M	N_r	G_r	**Mass** G_r	Qh	Ra	τ $(Cu - H_20)$
0.5	0.6	1.5	1.5	2	2	0.5	1.5	0.5313
1	0.6	1.5	1.5	2	2	0.5	1.5	-0.4559
1.5	0.6	1.5	1.5	2	2	0.5	1.5	-1.2996
2	0.6	1.5	1.5	2	2	0.5	1.5	-2.1782
0.5	**0**	1.5	1.5	2	2	0.5	1.5	2.8917
0.5	**0.2**	1.5	1.5	2	2	0.5	1.5	6.5405
0.5	**0.7**	1.5	1.5	2	2	0.5	1.5	0.5116
0.5	**1.2**	1.5	1.5	2	2	0.5	1.5	0.3835
0.5	0.6	**0**	1.5	2	2	0.5	1.5	1.1618
0.5	0.6	**1**	1.5	2	2	0.5	1.5	0.7247
0.5	0.6	**2**	1.5	2	2	0.5	1.5	0.3430
0.5	0.6	**3**	1.5	2	2	0.5	1.5	-0.0607
0.5	0.6	1.5	**1**	2	2	0.5	1.5	0.5034
0.5	0.6	1.5	**2**	2	2	0.5	1.5	0.5770
0.5	0.6	1.5	**3**	2	2	0.5	1.5	0.7820
0.5	0.6	1.5	1.5	**2**	**2**	0.5	1.5	0.5313
0.5	0.6	1.5	1.5	**5**	**5**	0.5	1.5	3.1838
0.5	0.6	1.5	1.5	**7**	**7**	0.5	1.5	4.9522
0.5	0.6	1.5	1.5	**11**	**11**	0.5	1.5	8.4889
0.5	0.6	1.5	1.5	2	2	**-0.75**	1.5	1.1006
0.5	0.6	1.5	1.5	2	2	**-0.5**	1.5	0.9190
0.5	0.6	1.5	1.5	2	2	**0**	1.5	0.6805
0.5	0.6	1.5	1.5	2	2	**1**	1.5	0.4299
0.5	0.6	1.5	1.5	2	2	**2**	1.5	0.3023
0.5	0.6	1.5	1.5	2	2	0.5	**1**	0.3365
0.5	0.6	1.5	1.5	2	2	0.5	**2**	0.7261
0.5	0.6	1.5	1.5	2	2	0.5	**3**	1.1157
0.5	0.6	1.5	1.5	2	2	0.5	**4**	1.5053

4. Validation

Table 6: The current study's Sherwood number is compared to that of Reddy and Raju [30].

S_c	K_r	**Sherwood number (Reddy and Raju)**	**Sherwood number(Present study)**
0.60	0.04	0.6376	0.6376
0.22	0.04	0.2546	0.2546
0.22	0.00	0.22	0.22
0.78	0.04	0.8181	0.8181
0.22	0.02	0.2385	0.2385

Table 6 shows how the Sherwood number from our study compares to what Reddy and Raju found [30]. In this study, the Sherwood numbers for $S = 1$ and are well correlated with those of Reddy and Raju [30].

5. Conclusion

In this work, analytical and numerical investigations are carried out for transient, natural convection MHD nanofluid flow over an infinitely long, moving vertical plate. The analysis considers uniform suction, chemical reaction, and a nonlinear thermal boundary condition. The governing equations are solved using the perturbation method. The influence of various physical parameters – such as the heat generation/absorption parameter and the radiation absorption parameter – is examined and validated

through graphical and tabulated results. Based on the findings of this study, the following conclusions are drawn.

- The non-dimensional velocity drops with increasing values of solid volume fraction (ϕ), heat generation/absorption parameter (Qh), Magnetic parameter (M), suction parameter (S), and chemical reaction parameter (K_r) while the non-dimensional velocity rises with increasing values of radiation absorption parameter (Ra), Grashof number (G_r), mass Grashof number (G_m), and thermal radiation (N_r).
- The temperature drops with increasing values of solid volume fraction (ϕ), heat generation/ absorption parameter (Qh), suction parameter (S), and chemical reaction parameter (Kr) while the temperature rises with increasing values of radiation absorption parameter (Ra), and thermal radiation (Nr).
- As the values of the chemical reaction parameter (Kr) and the suction parameter (S) get higher, the concentration decreases.
- As the values of the chemical reaction parameter (Kr) and the suction parameter (S) improve, the Sherwood number also climbs.
- As the values of sucction (S), chemical reaction (K_r), and heat generation/absorption (Qh) parameters elevate, the Nusselt number increases; as the levels of radiation absorption (Ra) and thermal radiation (N_r) elevate, the Nusselt number declines.
- The shear stress decreases as the suction parameter (S), chemical reaction parameter (K_r), heat generation/absorption parameter (Qh), and magnetic parameter (M) increase. In contrast, shear stress rises with higher values of the Grashof number (G_r), the modified Grashof number (G_m), the radiation absorption parameter (Ra), and the thermal radiation parameter (N_r).

Acknowledgments

The authors thank the management of REVA University for their support in carrying out this research work.

References

1. Arulmozhi, S., Sukkiramathi, K., Santra, S. S., Edwan, R., Fernandez-Gamiz, U., & Noeiaghdam, S. (2022). *Results in Engineering*, 14, 100394.
2. Prasad, P. D., Kumar, R. K., & Varma, S. V. K. (2018). *Ain Shams Engineering Journal*, 9(4), 801-813.
3. Reddy, P. Y. (2021). *Turkish Journal of Computer and Mathematics Education (TURCOMAT)*, 12(10), 4412-4426.
4. Rajesh, V., Mallesh, M. P., & Sridevi, C. (2015). *Procedia Engineering*, 127, 901-908.
5. Rajesh, V., Sheremet, M. A., & Öztop, H. F. (2021). *Case Studies in Thermal Engineering*, 28, 101557.
6. Kumaresan, E., Kumar, A. V., & Kumar, B. R. (2017, November). *In IOP Conference Series: Materials Science and Engineering* (Vol. 263, No. 6, p. 062018). IOP Publishing.
7. Pavar, P., Krishna, L. H., & Reddy, M. S. (2020, July). *In AIP Conference Proceedings* (Vol. 2246, No. 1). AIP Publishing.
8. Das, S., & Jana, R. N. (2015). *Alexandria Engineering Journal*, 54(1), 55-64.
9. Sobamowo, M. G. (2018). *International Journal of Chemical Engineering*, 2018.
10. Arifuzzaman, S. M., Khan, M. S., Islam, M. S., Islam, M. M., Rana, B. M. J., Biswas, P., & Ahmmed, S. F. (2017). *Frontiers in Heat and Mass Transfer*, 9, 25.
11. Prakash, J., Vijaya Kumar, A. G., Madhavi, M., & K Varma, S. V. (2014). *Applications and Applied Mathematics: An International Journal (AAM)*, 9(1), 10.
12. Nayan, Asmahani, et al. *Journal of Advanced Research in Fluid Mechanics and Thermal Sciences* 92.1 (2022): 51-64.
13. Krishna, M. V., Ahamad, N. A., & Chamkha, A. J. (2021). *Ain Shams Engineering Journal*, 12(3), 3043-3056.
14. Haq, S. U., Khaliq, H., Jan, S. U., Alqahtani, A. M., Khan, I., & Alam, M. N. (2022). *Journal of Mathematics*, 2022.

15. Krishna, M. V., Ahamad, N. A., & Chamkha, A. J. (2021). *Ain Shams Engineering Journal*, 12(2), 2099-2109.

16. Anwar, T., Kumam, P., Shah, Z., Watthayu, W., & Thounthong, P. (2020). *Molecules*, 25(4), 854.

17. Rosaidi, N. A., Ab Raji, N. H., Ibrahim, S. N. H. A., & Ilias, M. R. (2022). *Journal of Advanced Research in Fluid Mechanics and Thermal Sciences*, 93(2), 37-49.

18. Zukri, N. Z. M., Ilias, M. R., Ishak, S. S., Osman, R., Makhatar, N. A. M., & Abd Rahman, M. N. (2023). *CFD Letters*, 15(7), 92-111.

19. Raghunath, K. (2023). *Journal of Nanofluids*, 12(3), 767-776.

20. Nadeem, S., Akhtar, S., & Abbas, N. (2020). *Alexandria Engineering Journal*, 59(3), 1847-1856.

21. El-Dabe, N. T., Gabr, M. E., Elshekhipy, A. E. A., & Zaher, S. A. (2020). *Thermal Science*, 24(2 Part B), 1311-1321.

22. Rahman, M., & Uddin, J. (2021). *Heat Transfer*, 50(8), 7879-7897.

23. Kumar, M. A., Reddy, Y. D., Rao, V. S., & Goud, B. S. (2021). *Case studies in thermal engineering*, 24, 100826.

24. Ameer Ahamad, N., Veera Krishna, M., & Chamkha, A. J. (2020). *Journal of Nanofluids*, 9(3), 177-186.

25. Rai, P., & Mishra, U. (2023). *CFD Letters*, 15(10), 93-109.

26. Raghunath, K., Ramana, R. M., Reddy, V. R., & Obulesu, M. (2023). *Journal of Nanofluids*, 12(1), 147-156.

27. Raju, K. V., Mohanaramana, R., Reddy, S. S., & Raghunath, K. (2023). *Communications in Mathematics and Applications*, 14(1), 237.

28. Reddy, Y. D., & Goud, B. S. (2023). *Results in Engineering*, 17, 100796.

29. Hossain, M. A., Khanafer, K., & Vafai, K. (2001). *International Journal of Thermal Sciences*, 40(2), 115-124.

30. Reddy, P., & Raju, M. C. (2017). *Bulletin of Pure & Applied Sciences-Mathematics and Statistics*, 36(2), 152-164.

6. Nomenclature

R	Radiation absorption	N_r	Thermal radiation
$c1$	Invariant species concentration	c_w	Surface species concentration
c_∞	Ambient species concentration	G_r	Thermal Grashof number
K_r	Chemical reaction parameter	c_p	Specific heat capacitance
g	Gravitational acceleration	G_m	Mass Grashof number
K	Permeability parameter	M	Magnetic parameter
B_0	Transverse magnetic effects	b_∞	Ambient temperature
S_c	Schmidt number	a_1	Velocity along the x-direction
b_w	Surface temperature	a_2	y axis component velocity
b_1	Fluid temperature	$t\prime$	Non-dimensional time
S	Suction parameter	v_0	Uniform suction
P_r	Prandtl number	u_0	Uniform velocity
Q	Heat generation/Heat absorption		

6.1. Greek symbols

ρ	Density
ω	Angular oscilation
α	Thermal diffusivity
γ	Kinematic viscosity
ϕ	Solid particle volume fraction
α_1	Stefan-Boltzmann constant
ϵ	emissivity parameter
β	Thermal expansion coefficient
μ	Dynamic viscosity

7. Appendix

$$m_4=\frac{\left(\Pr AS+\sqrt{(\Pr AS)^2+4E_1(\Pr Aiw+Q_h)}\right)}{2E_1},\quad B_2=-\frac{Ra}{E_1(s_1+is_2)^2-\Pr AS(s_1+is_2)-(\Pr Aiw+Q_h)},$$

$$m_2=\frac{\left(ScS+\sqrt{(ScS)^2+4(iw+Kr)Sc}\right)}{2},\ s_5=\frac{\sqrt{2}A_1S+\sqrt{(A_1S)^2+4E_2M\sin^2\theta+\frac{4E_2}{K}+\sqrt{\left[(A_1S)^2+4E_2M\sin^2\theta+\frac{4E_2}{K}\right]^2+16(E_2A_1w)^2}}}{2\sqrt{2}E_2},$$

$$m_5=\frac{\left(A_1S+\sqrt{(A_1S)^2+4E_2\left(M\sin^2\theta+\frac{1}{K}\right)}\right)}{2E_2},\quad m_1=\frac{\left(ScS+\sqrt{(ScS)^2+4ScKr}\right)}{2},\quad B_1=-\frac{Ra}{E_1{m_1}^2-\Pr ASm_1-Q_h},$$

$$m_3=\frac{\left(\Pr AS+\sqrt{(\Pr AS)^2+4E_1Q_h}\right)}{2E_1},\quad B_3=-\frac{E_3Gr(1-B_1)}{E_2{m_3}^2-A_1Sm_3-\left(M\sin^2\theta+\frac{1}{K}\right)},\quad m_6=\frac{\left(A_1S+\sqrt{(A_1S)^2+4E_2\left(M\sin^2\theta+\frac{1}{K}+Aiw\right)}\right)}{2E_2},$$

$$B_4=-\frac{E_3GrB_1}{E_2{m_1}^2-A_1Sm_1-\left(M\sin^2\theta+\frac{1}{K}\right)},\quad B_7=-\frac{E_3GrB_2}{E_2(s_1+is_2)^2-A_1S(s_1+is_2)-\left(M\sin^2\theta+\frac{1}{K}+A_1iw\right)},$$

$$B_5=-\frac{E_4Gm}{E_2{m_1}^2-A_1Sm_1-\left(M\sin^2\theta+\frac{1}{K}\right)},$$

$$s_3=\frac{\sqrt{2}\Pr AS+\sqrt{(\Pr AS)^2+4E_1Q_h+\sqrt{\left[(\Pr AS)^2+4E_1Q_h\right]^2+16(E_1\Pr Aw)^2}}}{2\sqrt{2}E_1},\ B_8=-\frac{E_4Gm}{E_2(s_1+is_2)^2-A_1S(s_1+is_2)-\left(M\sin^2\theta+\frac{1}{K}+A_1iw\right)},$$

$$s_1=\frac{\sqrt{2}ScS+\sqrt{(SSc)^2+4ScKr+\sqrt{\left[(SSc)^2+4ScKr\right]^2+16Sc^2w^2}}}{2\sqrt{2}},\ B_6=-\frac{E_3Gr(1-B_2)}{E_2(s_3+is_4)^2-A_1S(s_3+is_4)-\left(M\sin^2\theta+\frac{1}{K}+A_1iw\right)},$$

$$s_2=\frac{\sqrt{2}Scw}{\sqrt{(SSc)^2+4ScKr+\sqrt{\left[(SSc)^2+4ScKr\right]^2+16Sc^2w^2}}},$$

$$s_6=\frac{\sqrt{2}A_1w}{\sqrt{(A_1S)^2+4E_2M\sin^2\theta+\frac{4E_2}{K}+\sqrt{\left[(A_1S)^2+4E_2M\sin^2\theta+\frac{4E_2}{K}\right]^2+16(E_2A_1w)^2}}},$$

$$s_4=\frac{\sqrt{2}\Pr Aw}{\sqrt{(\Pr AS)^2+4E_1Q_h+\sqrt{\left[(\Pr AS)^2+4E_1Q_h\right]^2+16(E_1\Pr Aw)^2}}}.$$

Akhil A. M.,
https://orcid.org/0009-0002-7790-3104
Department of Mathematics,
School of Applied Sciences,
REVA University,
Bengaluru 560064,
Karnataka, India.
E-mail address: kalal.akhil@outlook.com

and

Sreegowrav K. R.,
https://orcid.org/0000-0003-2069-8402
Department of Mathematics,
School of Applied Sciences,
REVA University
Bengaluru 560064
Karnataka,
India.
E-mail address: gowrav.86@gmail.com